Short Term Transversally Isotropic Creep of Plates Under Static and Periodic Loading

Holm Altenbach, Dmitry Breslavsky, Volodymyr Mietielov and Oksana Tatarinova

Abstract The statement and solution method of the two-dimensional problem of orthotropic creep under static and periodic loadings are presented. Experimental investigations of short-term deformation under uni-axial and plane stress states are carried out. Short-term creep curves were obtained for uni-axial specimens and plates with holes. Constitutive equations are developed for steel characterized by the first stage of unsteady creep with orthotropic properties under static and periodic loading. The calculation method in general was verified by comparing numerical and experimental results under the uni-axial and plane stress states.

Keywords Short-term creep · Orthotropic properties · Plane stress state · FEM · Experimental investigations

1 Motivation

Creep in metallic materials can occur at all temperatures and stress levels. As it was pointed out by Lemaitre and Chaboche [1], some alloys exhibit visco-plasticity (creep) at room temperatures (300 K), despite the fact that their melting temperatures can reach 1400 K.

H. Altenbach
Institut für Mechanik, Fakultät für Maschinenbau, Otto-von-Guericke-Universität Magdeburg, Universitätsplatz 2, 39106 Magdeburg, Germany
e-mail: holm.altenbach@ovgu.de

D. Breslavsky (✉) · V. Mietielov · O. Tatarinova
Department of Computer Modeling of Processes and Systems, National Technical University 'Kharkiv Polytechnic Institute', 2 Kyrpychova str., Kharkiv 61002, Ukraine
e-mail: brdm@kpi.kharkov.ua

V. Mietielov
e-mail: vometel@gmail.com

O. Tatarinova
e-mail: ok.tatarinova@gmail.com

K. Naumenko and M. Krüger (eds.), *Advances in Mechanics of High-Temperature Materials*, Advanced Structured Materials 117,
https://doi.org/10.1007/978-3-030-23869-8_9

With a significant level of stress, which in most cases exceeding the yield limit, and at room temperature, varying in time strains can reach significant values in structural steels. Because of the general rather high level of stresses, creep cannot run too long: either tertiary creep occurs with damage increase, resulting in fracture, or saturation occurs, at which the creep rate drops significantly. In both considered cases, the so-called short-term creep takes place.

Rabotnov and Mileiko [2] define short-term creep as a process of metal creep when a significant deformation, that limits the service function of the structural element and runs over a relatively short period of time. The authors emphasize that under such a significant stress the strain value 5% can be accepted. In the case of short-term creep, the deformation time is from tens to 1000 s. In [2] is noted, that approaches to the solution of short-term creep problems should be applied in the cases where the effect of sufficiently significant loads presents within a short time, and the accumulated creep strains are commensurate with instantaneous elastic-plastic deformations.

Examples of experimental studies of short-term creep as well as methods of its numerical simulation are given in [2–6] among others. As in [2] is emphasized, the models and methods traditionally used in creep calculations can also be used for the description of short-term processes. In this case, in almost all situations, the use of numerical methods of calculation is necessary.

In many cases, short-term creep occurs during cyclic deformation at low and room temperatures. In [7, 8] the results of experimental studies of cyclic creep at room temperatures of titanium alloys are considered. In [9] the similar behavioir of carbon steels was studied. Short-time creep under vibration loading, which leads to processes of dynamic creep in materials [3], was studied for alloys of non-ferrous metals and solders [10, 12, 13] as well as and for heat-resistant alloys [11].

In various technological processes due to the non-uniform mechanical actions, materials with anisotropic mechanical properties, including creep properties, are obtained. When rolling sheet materials, transversal isotropy of the plasticity and creep properties is often realized [14–16]. The models of Hill, Malinin – Khazhinsky and others are used for its description [1, 3, 4, 15, 16].

Also in technological processes sheet materials are subjected to the joint action of static and periodically (i.e. cyclically with the same cycle shape) varying loads. For the case of the same loading cycles for solving the initial-boundary value problem and formulating the governing equations, it is effective to use the multi-scale method with subsequent averaging over the period of stress variation. In [17, 18] this approach was applied to materials with isotropic creep properties, and in [19] a model for describing creep and damage of transversely isotropic materials is presented.

The problem statement describing the creep of transversally isotropic materials under conditions of a plane stress state and periodic loading is presented in this chapter. The formulation of the method for solving initial-boundary value problems based on using the methods of asymptotic expansions and averaging on a time period is given. The govering system of differential equations is solved using the finite element and difference methods in the time domain. The cases of static and combined static and periodically varying loading under uniaxial and two-dimensional plane stress state are considered. The results of an experimental study of the creep of

specimens and plates with holes allow verifying the constitutive equations and the calculation method.

2 Problem Statement and Method of Solution

Let us consider the mathematical statement of a two-dimensional creep problem for the area Ω with boundary curve Γ. The Cartesian coordinate system x_i ($i = 1, 2$) is used. We assume that the displacements $u_i|_{\Gamma_1} = \tilde{u}_i$ are specified on the part of the boundary Γ_1. The part of the boundary Γ_2 is loaded by tractions $p_i(x,t)$, and we do not consider the volume forces. The elastic and plastic properties of the material are considered as isotropic as well as the creep properties as transversally isotropic. The case of constant temperature is assumed.

We apply the Lagrange approach and the case of small strains is considered. The following notations are used: $\mathbf{u} = \mathbf{u}(x_i, t)$ is the displacement vector, $\boldsymbol{\varepsilon} = \boldsymbol{\varepsilon}(x_i, t)$, $\boldsymbol{\varepsilon}^{pl} = \boldsymbol{\varepsilon}^{pl}(x_i, t)$, $\boldsymbol{\varepsilon}^{c} = \boldsymbol{\varepsilon}^{c}(x_i, t)$ are the tensors of total strains, plastic and creep strains, respectively; $\boldsymbol{\sigma} = \boldsymbol{\sigma}(x_i, t)$ is the stress tensor, t denotes the time variable. The basic system of equations of the creep theory for the two-dimensional case has the following form [1]

$$\begin{gathered}\sigma_{ij,j} = \gamma \ddot{u}_i; \sigma_{ij} n_j = p_i(x); x \in \Gamma_2 \\ \varepsilon_{ij} = \tfrac{1}{2}\left(u_{i,j} + u_{j,i}\right), x \in \Omega; u_i|_{\Gamma_1} = \tilde{u}_i; x \in \Gamma_1; i, j = 1, 2 \\ \sigma_{ij} = C_{ijkl}\left(\varepsilon_{ij} - \varepsilon_{ij}^{pl} - \varepsilon_{ij}^{c}\right); \mathbf{u}(x_i, 0) = \mathbf{u}_0(x);\ \varepsilon_{ij}^{c}(x_i, 0) = 0.\end{gathered} \tag{1}$$

Here, $\mathbf{n}(n_1,n_2)$ is the unit vector of the normal to the contour, γ is the density of the material. The system (1) has to be added by a creep law.

The initial conditions are presented by the vector $\mathbf{u_0}$, determined by the solution of the system (1) in the initial elastic ($\boldsymbol{\varepsilon}^{pl} = \boldsymbol{\varepsilon}^{c} = 0$) or elastic-plastic ($\varepsilon^{c} = 0$) stress-strain states.

As is known [20], the most effective way for solving the problem is the expansion of the time-varying load component acting on the part of the contour Γ_2, in the Fourier series and subsequent representation of $p_i(x,t)$ in the following form

$$p_i(x_i, t) = p_i^0(x_i) + p_i^{\max}(x_i)\Psi^{(1)}(t), i = 1, 2. \tag{2}$$

Here the following notations are used:
$p_i^0(x_i)$ is the time-independent load component; $\Psi^{(1)}(t) = \sum_{k=1}^{\infty} \Psi_k = \sum_{k=1}^{\infty} A_k \sin(\tilde{p}_k t + \beta_k)$ is the component of the load, which varies in time with the period T;

$$\Psi_k(t) = a_k \cos\left(\frac{2\pi k}{T_p} t\right) + b_k \sin\left(\frac{2\pi k}{T_p} t\right);$$

$$A_k = \left(a_k^2 + b_k^2\right)^{1/2};\ \tilde{p}_k = \frac{2\pi k}{T_p};\ \beta_k = \mathrm{arctg}(a_k/b_k);$$

a_k, b_k are coefficients of the Fourier series; p_i^{max} are amplitude values of load components.

Following the approaches proposed in [17–19], the solution of the system (1), taking into account the acting variable load (2), can be found by the application of the method of multi-time scales with subsequent time averaging [21]. According to these approaches, the solution of system (1) can be determined by the solution of such a similar system, in which only unvaried load is taking into account. In this case, the amplitude values of the components of the stress-strain state, which are determined by the action of the variable component $\Psi^{(1)}$, are included into the creep law of special form.

To determine the components of the strain-stress state under creep, which occurs as a result of the action of constant and periodically varying loads, the solution of the following system of equations is necessary:

$$\begin{gathered}
\sigma_{ij,j} = 0, \quad x_i \in \Omega;\ i = 1, 2 \\
\sigma_{ij} n_j = p_i^0, \quad x_i \in \Gamma_2; \\
\sigma_{ij} = C_{ijkl}\left(\varepsilon_{ij} - \varepsilon_{ij}^{pl} - \varepsilon_{ij}^{c}\right);\ \varepsilon_{ij} = \tfrac{1}{2}\left(u_{i,j} + u_{j,i}\right),\ x \in \Omega;\ u_i|_{\Gamma_1} = \tilde{u}_i;\ x \in \Gamma_1; \\
\mathbf{u}(x_i, 0) = \mathbf{u}_0(x); \quad \varepsilon_{ij}^{c}(x_i, 0) = 0.
\end{gathered} \tag{3}$$

Now let us consider the creep law of transversally-isotropic material for the case of primary creep. For the case of static load, it is given in [19, 22]:

$$\dot{\boldsymbol{\varepsilon}}^c = \tilde{B}\left(\boldsymbol{\varepsilon}_{vM}^c\right)^{-\alpha} \boldsymbol{\sigma}_v^{n-1} \left[\overline{B}\right] \boldsymbol{\sigma}. \tag{4}$$

The plane stress state is considered, and the following notations are introduced: $\boldsymbol{\varepsilon}^c$ is the vector of creep strain; $\boldsymbol{\sigma}$ is stress vector; $\left[\overline{B}\right]$ is a matrix containing creep constants for transversally isotropic material in the case of two-dimensional stress state. b_{ijkl} are the components of the tensor containg the creep properties of the material; $\varepsilon_{vM}^c = \sqrt{\frac{2}{3}\varepsilon_{ij}^c \varepsilon_{ij}^c}$ is the von Mises creep strain; $\sigma_v = \boldsymbol{\sigma}^T [B] \boldsymbol{\sigma}$ is the equivalent stress, which is a common invariant of the stress tensor and the tensor of material parameters

$$\sigma_{\mathbf{v}} = \left(b_{1111}\sigma_{11}^2 + 2b_{1122}\sigma_{11}\sigma_{22} + b_{2222}\sigma_{22}^2 + 4b_{1212}\sigma_{12}^2\right)^{1/2};$$

$\tilde{B}$, α, n are creep parameters.

Equation (4) is formulated for the case when the main axes of anisotropy (transversal isotropy in this case) coincide with the axes of the Cartesian coordinate system. In the case when they are rotated one to another by the angle θ, the relations (3) can be modified by converting the components of stress tensors and creep strain rates. In

this case, the matrix of the coordinate transformation, which is dependent from the angle θ [23], should be added to the right-hand side of (3) as a factor.

Let us present the way of the creep equation deriving for the case of periodic loading [22]. First, we consider the case of uniaxial stress state when a combined cyclic stress $\sigma = \sigma^0 + \sigma^1$ operates on a point (or specimen). Here, the constant stress denotes as σ^0 and stress σ^1 varies with the cyclic frequency $f_1 = 1/T_p$ over the period of the cycle T_p ($f_1 \ll 1$ Hz). In the general case, the stress σ^1 is determined by the parameters of the operating cycle with amplitude, which periodically increases and decreases.

We present the form of the stress σ^1 by expansions in the periodic Fourier series with coefficients a_k and b_k ($k = 1, 2, \ldots$):

$$\sigma^1 = \sigma^{\max}\left(\sum_{k=1}^{\infty}\left(a_k \cos\left(\tfrac{2\pi k}{T_p}t\right) + b_k \sin\left(\tfrac{2\pi k}{T_p}t\right)\right)\right) = \sum_{k=1}^{\infty}\sigma^{ak}\sin\left(\tfrac{2\pi k}{T_p}t + \beta_k\right),$$
$$\sigma^{ak} = \sqrt{\left(\sigma^{\max}a_k\right)^2 + \left(\sigma^{\max}b_k\right)^2},\ \beta_k = \operatorname{arctg}(a_k/b_k), \tag{5}$$

For a combined load, the law of periodic stress varying can be written in such form:

$$\sigma = \sigma^0 + \sigma^1 = \sigma^0\left(1 + \sum_{k=1}^{\infty} M_k \sin\left(\frac{2\pi k}{T_p}t + \beta_k\right)\right), \tag{6}$$

where $M_k = \frac{\sigma^{ak}}{\sigma^0}$ are the stress cycle amplitude coefficients, $\sigma^0 \neq 0$.

Let us rewrite Eq. (4) for a uniaxial stress state:

$$\dot{\varepsilon}^c = \tilde{B}\left(\varepsilon^c\right)^{-\alpha}\sigma^n. \tag{7}$$

We will use the method of multi- (two in the considered problem) scales and asymptotic expansion of the basic unknowns on small parameter $\mu = T_p/t$. We apply this approach to Eq. (7). Let us introduce the process of creep strain growth in two time scales (slow t and fast $\xi = \tau/T_p$, where $\tau = t/\mu$) using the form of asymptotic expansion:

$$\varepsilon^c \cong \varepsilon^{c0}(t) + \mu\varepsilon^{c1}(\xi), \tag{8}$$

where $\varepsilon^{c0}(t)$, $\varepsilon^{c1}(\xi)$ are the functions corresponding to the basic process of creep in slow (0) and fast (1) scales of time. We limit us only by the first approximation, assuming in (8) the members with higher degrees of the parameter μ are too small. Further, we can obtain

$$\left(\varepsilon^{c0} + \mu\varepsilon^{c1}\right)^{\alpha} = \varepsilon^{c0}\left(1 + \mu\frac{\varepsilon^{c1}}{\varepsilon^{c0}}\right)^{\alpha} \cong \varepsilon^{c0}. \tag{9}$$

Taking into account the dependence of the creep strain only on the "slow" time [17, 18], after averaging over a period on the "fast" scale, we obtain:

$$\left\langle \varepsilon^{c0}(\xi) \right\rangle = \int_0^1 \varepsilon^{c0}(t)\, d\xi \cong \varepsilon^{c0}(t), \left\langle \varepsilon^{c1}(\xi) \right\rangle = \int_0^1 \varepsilon^{c1}(\xi) d\xi \cong 0. \tag{10}$$

Thus, using the method of asymptotic expansion with a subsequent averaging over the cyclic load period (10), for a uniaxial stress state we obtain the law of creep during periodic loading for materials with transversally isotropic creep properties:

$$\dot{\varepsilon}^c = \tilde{B}\left(\sigma^0\right)^n K\left(M^{(n)}\right)\left(\varepsilon^c\right)^{-\alpha}, \tag{11}$$

where $K(M^{(n)}) = \int_0^1 \left(1 + \sum_{k=1}^{\infty} M_k^{(n)} \sin(2\pi k\xi + \beta_k)\right)^n d\xi$, $M^{(n)} = \frac{\sigma^{ak}}{\sigma^0}$ is the coefficient of asymmetry of the stress cycle.

We generalize Eq. (11) for the case of a complex stress state, proceeding from the traditional postulate of creep theory, which establishes the correspondence between the values of stresses and strain rates at uniaxial and complex stress states [1, 3]. Then Eq. (4), taking into account (11), is rewritten in the following form:

$$\dot{\varepsilon}^{c0} = \tilde{B}\left(\varepsilon_{vM}^{c0}\right)^{-\alpha} \sigma_v^{0n-1} K\left(M^{(n)}\right)[\overline{B}]\sigma^0 \tag{12}$$

where $\boldsymbol{\varepsilon}_{vM}^{c0} = \sqrt{\frac{2}{3}\varepsilon_{ij}^{c0}\varepsilon_{ij}^{c0}}$ is the von Mises strain and $\boldsymbol{\sigma}_v^0 = \boldsymbol{\sigma}^{0T}[B]\boldsymbol{\sigma}^0$ is the equivalent stress, which is a common invariant of the stress tensor and the tensor of material parameters. It is determined by the components of the stress tensor in the "slow" process; $\mathrm{M}^{(n)} = \frac{\sigma_v^{ak}}{\sigma_v^0}$ is the stress cycle asymmetry coefficient; $\sigma_{\mathrm{v}}^{\mathrm{ak}} = \boldsymbol{\sigma}^{akT}[B]\boldsymbol{\sigma}^{ak}$ is an invariant of amplitude stresses. In the widespread case, when the components of the stress tensor are varyied in time by stepped law, the Eq. (5) will take the following form:

$$\begin{gathered}
\boldsymbol{\sigma} = \boldsymbol{\sigma}^0 + \boldsymbol{\sigma}^1 = \boldsymbol{\sigma}^0\left(1 + \sum_{k=1}^{\infty} M_k \sin\left(\frac{2\pi k}{T_p}t + \beta_k\right)\right), \\
\boldsymbol{\sigma}^{ak} = \sqrt{\left(\boldsymbol{\sigma}^{\max} a_k\right)^2 + \left(\boldsymbol{\sigma}^{\max} b_k\right)^2}, \beta_k = \operatorname{arctg}(a_k/b_k), \\
a_k = \frac{1}{\pi k}\sin\left(\frac{2T_s}{T_p}\pi k\right), b_k = \frac{1}{\pi k}\left(1 - \cos\left(\frac{2T_s}{T_p}\pi k\right)\right).
\end{gathered} \tag{13}$$

Here T_s is the value of time of the action of the larger stress $\sigma^0 + \sigma^{max}$; T_p is the value of time of less stress σ^0 action.

As was obtained [17, 18], for the case of a plane stress state, the components of amplitude stress tensors are determined by the solution of the following system ($k = 1, 2, \ldots ..$)

$$\begin{gathered}\sigma_{ij,j}^{ak} = -\gamma(\tilde{p}_k)^2 u_i^{ak}, x_i \in \Omega; \\ \sigma_{ij}^{ak} n_j = p_i^{\max} A_k, \ x_i \in \Gamma_2; \\ \varepsilon_{ij}^{ak} = \frac{1}{2}\left(u_{i,j}^{ak} + u_{j,i}^{ak}\right) = C_{ijmn}\sigma_{mn}^{ak}, x_i \in \Omega; \\ u_i^{ak}(0) = 0, x_i \in \Gamma_1;\end{gathered} \tag{14}$$

By solution of the system (14), for each kth harmonic, the components of amplitude stresses can be found. This determines the coefficients included in the constitutive Eq. (11).

In the case when the initial von Mises stresses are greater than the yield limit of material, the problem of elastic-plastic deformation is necessary to solve in order to determine the initial conditions for the systems (1) or (3):

$$\begin{gathered}\sigma_{ij,j} = 0_i; \sigma_{ij} n_j = p_i(x); x \in \Gamma_2 \\ \varepsilon_{ij} = \frac{1}{2}\left(u_{i,j} + u_{j,i}\right), x \in \Omega; \ u_i|_{\Gamma_1} = \tilde{u}_i; x \in \Gamma_1; i = 1, 2 \\ \sigma_{ij} = C_{ijkl}\left(\varepsilon_{ij} - \varepsilon_{ij}^{pl}\right); \\ f\left(\sigma_{ij}\right) = \frac{3}{2} s_{ij} s_{ij} - \Phi\left(\int d\bar{\varepsilon}_i^{pl}\right)^2; \varepsilon_i^{pl} = \Phi\left(\int d\bar{\varepsilon}_i^{pl}\right); d\varepsilon_{ij}^{pl} = \frac{3}{2}\frac{d\bar{\varepsilon}_i^{pl}}{\sigma_i} s_{ij}.\end{gathered} \tag{15}$$

3 Numerical Solution

As a method of solution of systems (3), (14) and (15), the finite element method (FEM) is used. Applying the main approaches of FEM, we arrive to a system of differential equations [24] for a finite element

$$\left(\int_V [B]^T [C][B] dV\right)\dot{\mathbf{u}}^{\gamma} = \int_V [B]^T [C]\dot{\varepsilon}^{c\beta} dV + \int_{S_1} [N]^T \dot{\mathbf{p}} dS \tag{16}$$

$$\dot{\boldsymbol{\sigma}}^{\beta} = [C]\left(\dot{\boldsymbol{\varepsilon}}^{\beta} - \dot{\boldsymbol{\varepsilon}}^{c\beta}\right), \tag{17}$$

$$\dot{\boldsymbol{\varepsilon}}^{\beta} = [B]\dot{\mathbf{u}}^{\gamma}, \tag{18}$$

where $[B]$ is the deformation matrix of the element with number β; $[C]$ is the matrix containing elastic properties of the material (matrix of elasticity); $\mathbf{u}^{\boldsymbol{\gamma}}$ is the vector of the nodal displacements of the element, $\boldsymbol{\gamma}$ is a number of node; $\boldsymbol{\sigma}^{\beta}$, $\boldsymbol{\varepsilon}^{\beta}$ are the vectors of stress and strains in the element; $[N]$ is the matrix of shape functions values; $\boldsymbol{p}$ is a traction vector. The complete system of equations for the whole model is obtained by ensembling the element's stiffness matrices into the global stiffness matrix $[K]$ as well as the vector of nodal forces $\{F\}$ [25]. Finally, for creep problems it has the following form

$$[K]\dot{\mathbf{U}} = \dot{\mathbf{F}} + \dot{\mathbf{F}}^{\mathbf{C}}. \tag{19}$$

Here $\mathbf{U}$ is the global vector of nodal displacements; $\mathbf{F}^c$ is the vector obtained by the values of forces, caused by creep strains. The solution of system (14) is obtained for the values of the nodal displacements in the same way (without creep strains).

The considered finite element formulation was implemented into the software complex *FEM CREEP* [24] and used for calculations. In the calculations, a triangular three-node finite element with a linear approximation of the displacements per element was used. The obtained systems of differential Eq. (19) are solved by the predictor-corrector method of third order or by the Euler method [20]. According to the generally accepted problem statement [26] for integrating the physically nonlinear creep problems, at each time step the vector of creep strain rates $\dot{\boldsymbol{\varepsilon}}^c = \left(\dot{\varepsilon}^c_{11}, \dot{\varepsilon}^c_{22}, 2\dot{\varepsilon}^c_{12}\right)^T$ is calculated using the stress vector $\boldsymbol{\sigma} = (\sigma_{11}, \sigma_{22}, \sigma_{12})^{\mathrm{T}}$, obtained in the previous time step, and the creep law (11):

$$\dot{\boldsymbol{\varepsilon}}^c = \tilde{B}\left(\boldsymbol{\varepsilon}^c_{vM}\right)^{-\alpha}\sigma_v^{n-1}\left[\overline{B}\right]\boldsymbol{\sigma}. \tag{20}$$

We have added for the case of a static load and for the case of a periodic load the expression of the influence function:

$$\dot{\boldsymbol{\varepsilon}}^c = \tilde{B}\left(\varepsilon^c_{vM}\right)^{-\alpha}\sigma_v^{n-1}K\left(\mathrm{M}^{(n)}\right)\left[\overline{B}\right]\boldsymbol{\sigma} \tag{21}$$

At each integration step, the system of linear algebraic equations is solved by the Cholesky decomposition [25].

In many cases, the initial load value is such that the von Mises stress exceeds the yield limit and the strain vector in the finite element consists of elastic and plastic components:

$$\boldsymbol{\varepsilon} = \mathbf{e} + \boldsymbol{\varepsilon}^{pl}. \tag{22}$$

A schematic stress-strain diagram in one-dimensional case is shown at Fig. 1, where 1 corresponds to elastic strains, 2 to yield plateau and 3 to plastic strains with hardening.

To determine the values of the initial plastic strain components, the method known as "increment-initial strain" method [25] was used.

At first, let us consider the algorithm for materials with hardening (linear or power law), when the yield plateau is absent, $\varepsilon^{\Pi} = 0$, and after the first part of the curve the third occurs [4]. We apply the Hencky-von Mises theory [1]. According to this theory, we assume that the increment of the strain vector components $\{\Delta\boldsymbol{\varepsilon}\}^{pl} = \{\Delta\varepsilon_x, \Delta\varepsilon_y, \Delta\gamma_{xy}\}$ is proportional to the effective stress, and the factor depends on the growth of the effective stress σ_{vM}

$$\begin{bmatrix} \Delta\varepsilon_x^{pl} \\ \Delta\varepsilon_x^{pl} \\ \Delta\gamma_{xy}^{pl} \end{bmatrix} = \frac{3}{2}\frac{d\bar{p}_i}{\sigma_{vM}}\begin{bmatrix} 1 & 0 & 0 \\ 0 & 1 & 0 \\ 0 & 0 & 2 \end{bmatrix}\begin{bmatrix} s_x \\ s_y \\ s_{xy} \end{bmatrix}, \tag{23}$$

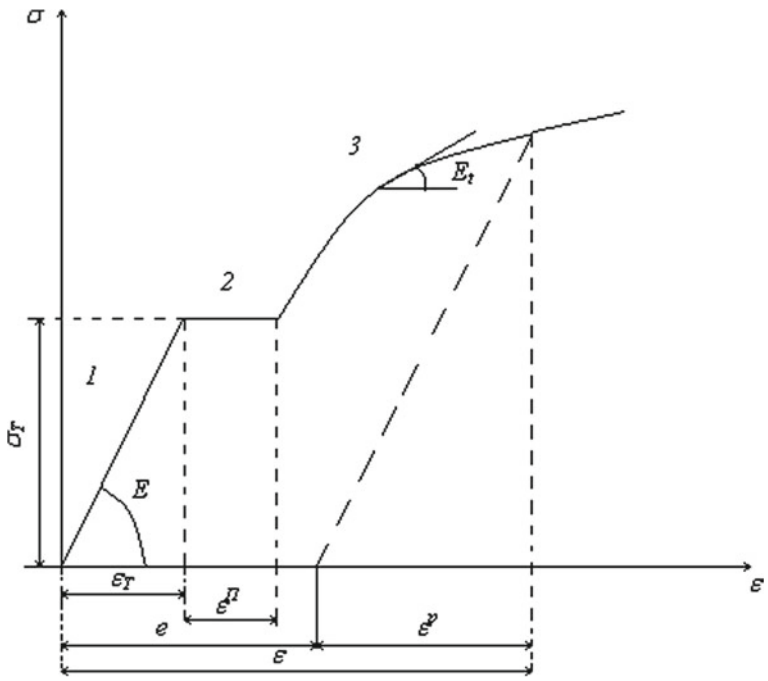

Fig. 1 Schematic stress-strain diagram

where $d\bar{p}_i = \frac{\sqrt{2}}{3}\sqrt{(\Delta\varepsilon_x^{pl} - \Delta\varepsilon_e^{pl})^2 + (\Delta\varepsilon_x^{pl})^2 + (\Delta\varepsilon_y^{pl})^2 + \frac{3}{2}(\Delta\gamma_{xy}^{pl})^2}$. Further we calculate the nodal forces that correspond to the plastic strains considered at the current stage $\Delta\boldsymbol{\varepsilon}^{pl}$, and a system of linear algebraic equations for a finite element is solved

$$\left(\int_V [B]^T[C][B]dV\right)\{\Delta u^\gamma\} = \int_V [B]^T[C]\left\{\Delta\varepsilon^{pl\beta}\right\}dV + \int_{S_1} [N]^T\{\Delta p\}dS \quad (24)$$

$$\left\{\Delta\sigma^\beta\right\} = [C]\left(\boldsymbol{\varepsilon}^\beta - \boldsymbol{\varepsilon}^{pl\beta}\right), \quad (25)$$

$$\boldsymbol{\varepsilon}^\beta = [B]\mathbf{u}^\gamma. \quad (26)$$

At each step the recalculation of the stiffness matrix of the element according to the stress-strain diagram (Fig. 1) with the correspondent tangent module E_t should be performed. It is considered [25, 26] that the load is added in small increment. The relations (24)–(26) are applied from the moment of approaching the von Mises stress σ_i the value of the yield limit σ_T. With each small load step, the required values of the strain components are calculated as

$$\boldsymbol{\varepsilon}_{ij}^{pl\beta} = \boldsymbol{\varepsilon}_{ij}^{pl\beta} + \Delta\boldsymbol{\varepsilon}_{ij}^{pl\beta} \tag{27}$$

The calculations are performed until the "moment" when the external load value is given by the conditions of the considered problem.

This algorithm can be modified for materials, which stress-strain diagram has a so-called "yield plateau". This behavior is classified as an ideal plastic solid [1, 4]. The problem is to determine the accumulated total strain in the solid at the "moment" when the accumulated value of the von Mises strain ε_{vM} is approached and the transition to the zone 3 of the diagram begins (Fig. 1). A direct iterative method is used for calculations [25]. This method is based on the sequence of approximations, which is presented for the uniaxial stress-strain state in this way

$$\begin{aligned} E(\sigma) &= E_0, \sigma < \sigma_T, \\ E(\sigma) &= \frac{E_0\varepsilon_0}{\varepsilon}, \sigma > \sigma_T. \end{aligned} \tag{28}$$

Here the index «0» indicates the current values on the yield plateu.

In the case of a biaxial stress state, the current (tangential) module $E(E_t)$ depends on the invariants of the strain or stress tensor. The algorithm for solving this can be formulated as follows:

1. The problem of "elastic" strains, described by the system (19) is considered. The components of the stress-strain state are determined using the initial values of the elastic modulus E and the Poisson's coefficient ν.
2. For each finite element new values of E and ν are determined, depending on the strain values obtained in the previous step (von Mises strains and stresses are used in Eq. (28)).
3. An "elastic" calculation again is made in which the parameters E and ν defined in the previous step are used.

Steps 2 and 3 are repeated until convergence is achieved, for example, for n and $n+1$ steps the condition $\left|\varepsilon_i^{n+1} - \varepsilon_i^n\right| < \delta$ is used.

For materials in which the stress-strain diagram after the yield plateau is of hardening type (Fig. 1), the algorithms considered are combined: after the calculation of the ideal plastic solid, the distribution of components of the stress-strain state is used as the initial values for calculations based on the hardening model.

4 Short-Term Creep of Uniaxial Specimens

To verify the developed method of calculation and constitutive equations, several experimental investigations were realized. Creep of uniaxial specimens and plates with holes under tension made from steel 3 (its chemical composition in %: 0.58 – 0.67 C, 0.22 – 0.45 Si, 0.5 – 0.9 Mn, max 0.02 S, max 0.03P, 0.08 – 0.15 V, the rest is Fe; closest analogues are A107 or USt 37–2) was considered. This steel is widely used

in manufacturing and in construction, for example, in form of complex profiles which was bent from it. This technological operation can run for a rather long time (tens of seconds) with a high level of stress. Steel sheets are produced by rolling, which leads to the transversal isotropy of the creep properties. Therefore, for computer simulation of technological processes it is necessary to have a proven method of calculation and constitutive equation that are implemented in the corresponding software.

The results of the experimental study at room temperature of uniaxial specimens from steel 3 under tension are given in [22]. In experiments with static loading 27 samples were tested at three stress levels: 378.7 MPa, 366.8 MPa and 352.3 MPa. All exceed the yield limit $\sigma_y = 295.8$ MPa. Specimens were cut from the sheets in three directions—along, across the rolling direction and at an angle of 45° to the lat one direction.

The results of the investigations confirmed the hypothesis of transversal isotropy of the creep properties of this material at room temperature. Then the parameter's values for Eq. (4) were determined. Its integrated form was used:

$$\varepsilon_i^c = b_i \sigma^m t^k. \tag{29}$$

where: $b_i = ((\alpha+1)B_i)^{\frac{1}{\alpha+1}}$, $i = 1, 2, 3$, $m = \frac{n}{\alpha+1}$, $k = \frac{1}{\alpha+1}$. After processing the experimental data, we obtained:

$m = 18.305$, $k = 0.1887$; $\left((\alpha+1)\tilde{B}\right)^{\frac{1}{\alpha+1}} = b_1 = 3.166.10^{-31}$ (10 MPa)$^{-m}$/h, $b_2 = 0.75b_1$, $b_3 = 0.42b_1$, $n = 96.99$, $\alpha = 4.3$, $b_{1111} = 6.9 \cdot 10^{-4}$, $b_{1122} = -3.45 \cdot 10^{-4}$, $b_{2222} = 6.7 \cdot 10^{-4}$, $b_{1212} = 1.85 \cdot 10^{-4}$, (10 MPa)$^{-2m/m+1}$/h$^{2/m+1}$.

As an example, the curves of static short-term creep for specimens which were cut in the rolling direction are presented in Fig. 2. Experimental data are presented by points. Solid lines correspond to calculated data. The curves are built for tensional stress values: curve 1: 378.7 MPa; curve 2: 366.8 MPa; curve 3: 352.3 MPa. In all cases, the difference between the experimental and estimated data did not exceed 15%.

Experiments were also carried out according to the stepped periodic loading program (Fig. 3).

In experiments, it was specified: $T_s = 60$ s. (0.0166 h), $T_p = 240$ s. (0.0066 h). Experiments were done for 10 load cycles (total time 2400 s.). The stress values were $\sigma = 352.3$ MPa, $\sigma^{max} = 26.4$ MPa. During the first 60 s in a cycle, the specimens were loaded with a stress $\sigma = 352.3$ MPa, then 180 s with the stress $\sigma = 378.7$ MPa. These stress values are the minimum and maximum load values used in static experiments.

The derived creep law for the periodic loading Eq. (11) was verified using comparison with the experimental curves. The calculation of the creep curves, which corresponds to the cycle load applied in the experiment, was performed by developed computer program based on C-language. The results of calculations are shown on Fig. 4. Here, curve 1 corresponds to the data for the specimens cutted in the longitudinal direction, curve 2: transversal direction; curve 3 at an angle of 45° to

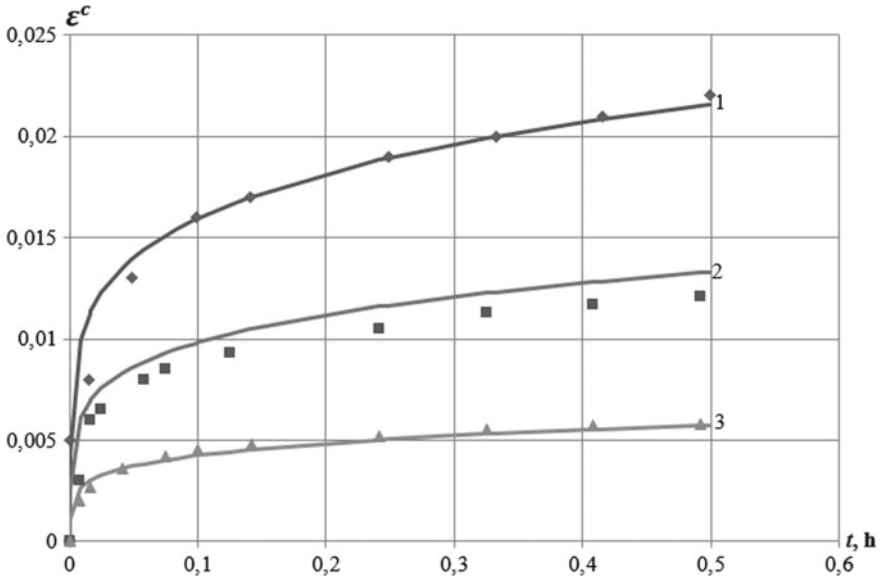

Fig. 2 Static loading. Comparison of numerical and experimental creep curves (specimens cutted in the rolling direction)

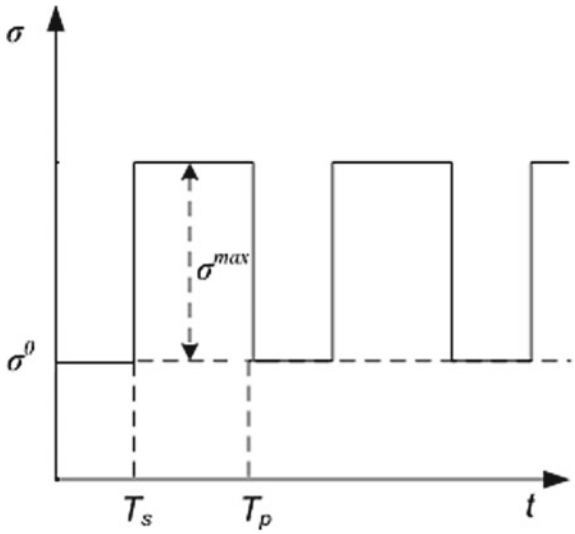

Fig. 3 Program of periodic loading

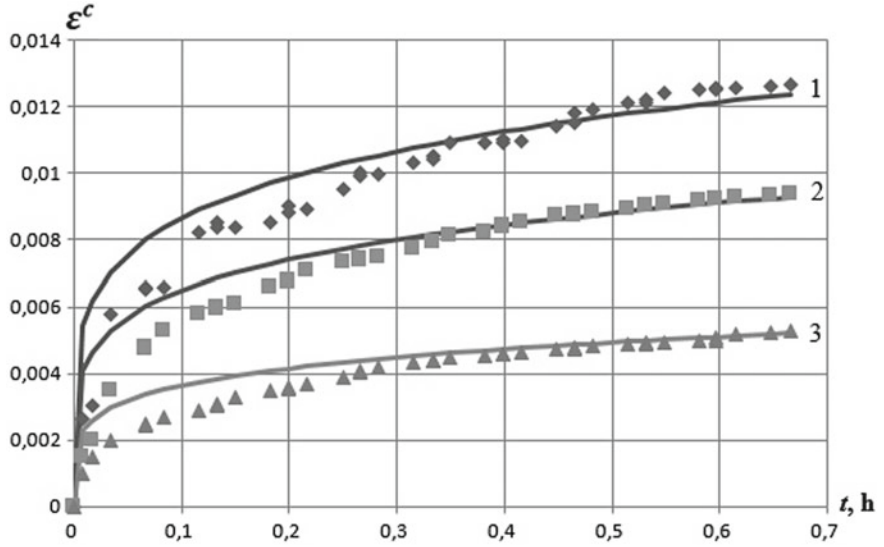

Fig. 4 Periodic loading. Comparison between calculated and experimental data

the rolling direction. Experimental data averaged by three specimens are marked by points, calculated data presented by solid curves.

Figure 4 shows that the proposed creep equations for the case of periodic stress action describe in a satisfactory manner the experimentally obtained curves starting from the 4–5th cycle. The maximum error is obtained in first cycles and is equal to 35%. This takes place because for a small number (1–3) of load cycles, where the value of the parameter μ cannot be considered as small, the averaged equation is not entirely correct. The greater number of load cycles, the less error. Its value in 4–10th cycles does not exceed 10%. It can be seen from the graphs that for the considered creep time the application of the developed averaged equation is acceptable: starting from the fourth load cycle, the difference in experimental and numerical results is insignificant.

The testing of the method's efficiency and the developed software for modeling of transversally isotropic creep under assumption of plane stress state was performed with numerical simulations of plane specimens cutted in different directions. In this case, the specimens are modeled as plane rectangles, loaded with a traction along the axis, which is parallel to their long side. Because the results of experiments were obtained on plane specimens from steel 3, the same typical location of FE models with orientation of 0°, 45° and 90° to the rolling direction was considered. Three FE schemes corresponding to the specified directions are shown in Fig. 5

All three FE models were used for calculations up to 0.5 h, which correspond to the time of the experiments. It was assumed in all calculations, that the models were loaded by tensile traction equal to 378.7 MPa.

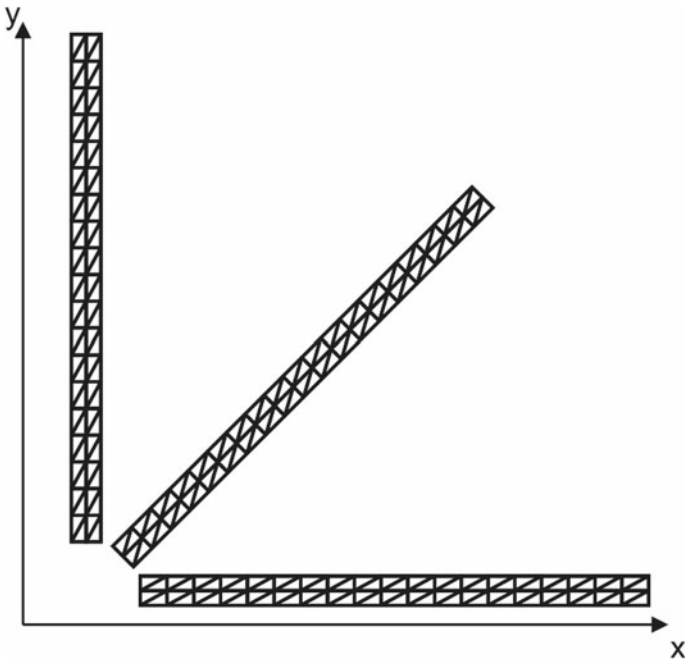

Fig. 5 The location of finite element models of specimens under tension

The results of calculations for the case of static load are presented in Figs. 6, 7 and 8, where the comparison of experimental (points), calculated by Eq. (4) (dotted lines) and FE results (solid lines) are presented. Figure 6 corresponds to the data for the rolling direction, Fig. 7—transverse direction; Fig. 8—at an angle of 45° to rolling direction. The results show that the calculated and FE data coincide with the accuracy of 1–2%, which demonstrates the correctness of all algorithms, including those related to the implementation of the creep law and time integration, and the entire software as a whole. Differences in experimental and FE data are the same as those when comparing them with the calculated ones.

Let us analyze now the results of the experimental data in the case of periodic loading with the results of numerical creep modeling with Eq. (11), which were obtained by asymptotic and averaging methods. We use the same FE models (Fig. 5). The results are presented in Figs. 9, 10 and 11. The numerical results are shown by solid lines and the experimental data by points.

The diagrams show that the developed software tool allows in general a satisfactorying modeling of creep processes at periodic loading in steel 3. The difference between experimental and numerical results does not exceed 10–15% for time domains which are after the first four loading cycles, which is similar to the prevoious static case. At low number of cycles (2–4) the error is 25–30%. For all three directions,

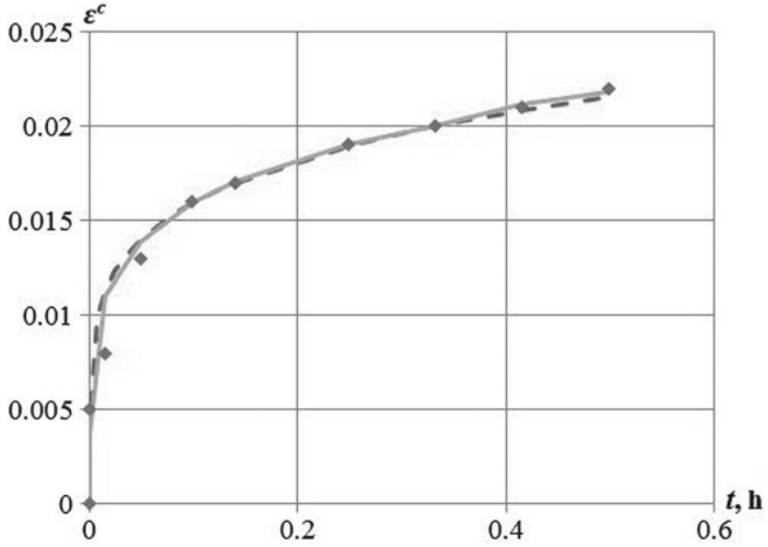

Fig. 6 Comparison of experimental, calculation and finite element data (rolling direction)

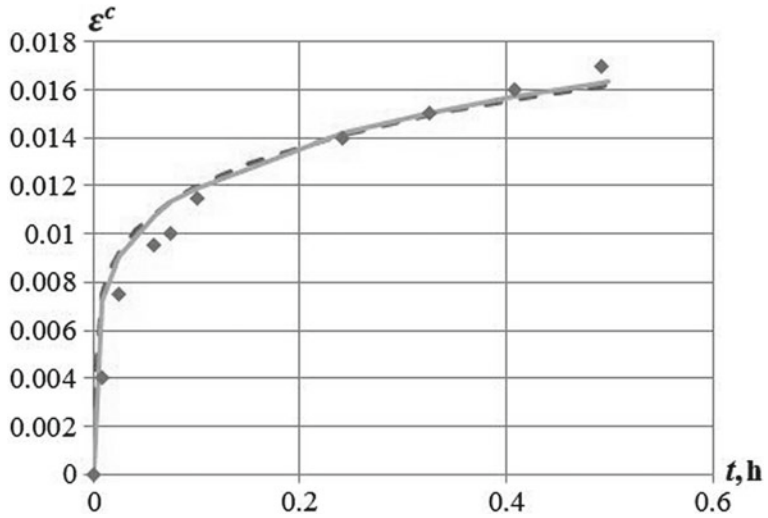

Fig. 7 Comparison of experimental, calculation and finite element data (transverse direction)

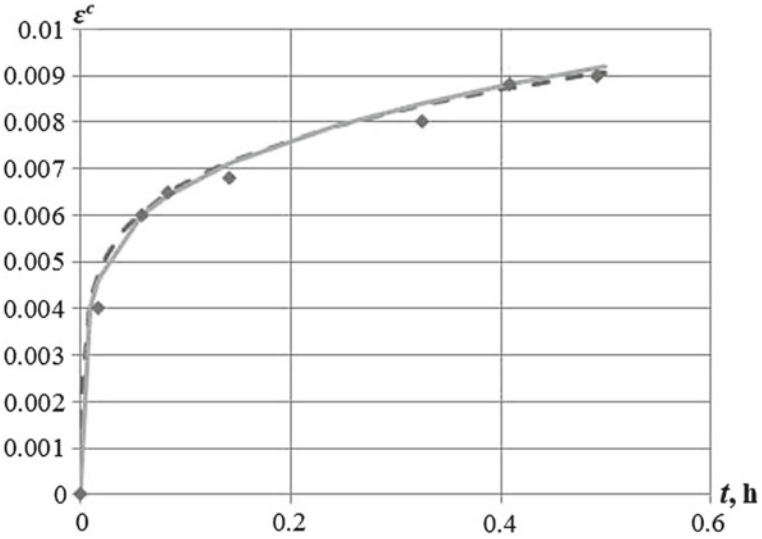

Fig. 8 Comparison of experimental, calculation and finite element data (direction at an angle of 45° to the rolling direction)

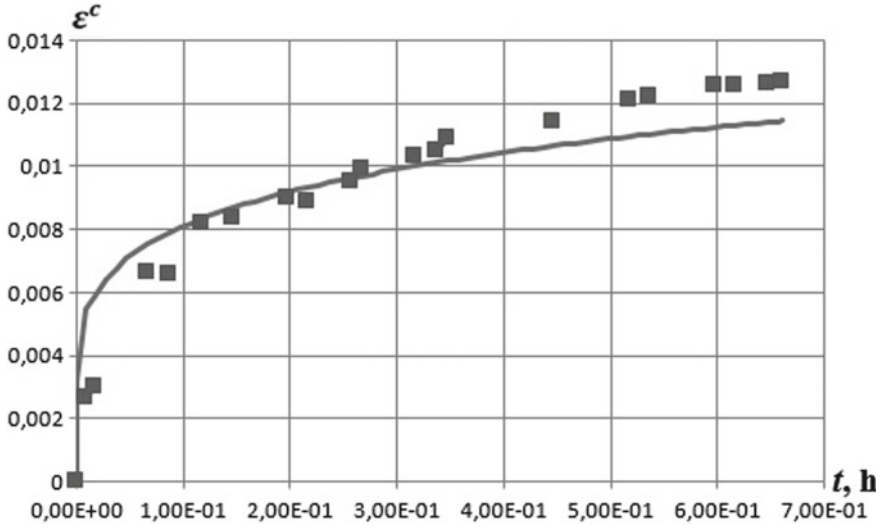

Fig. 9 Comparison of experimental and finite element results (periodic load, rolling direction)

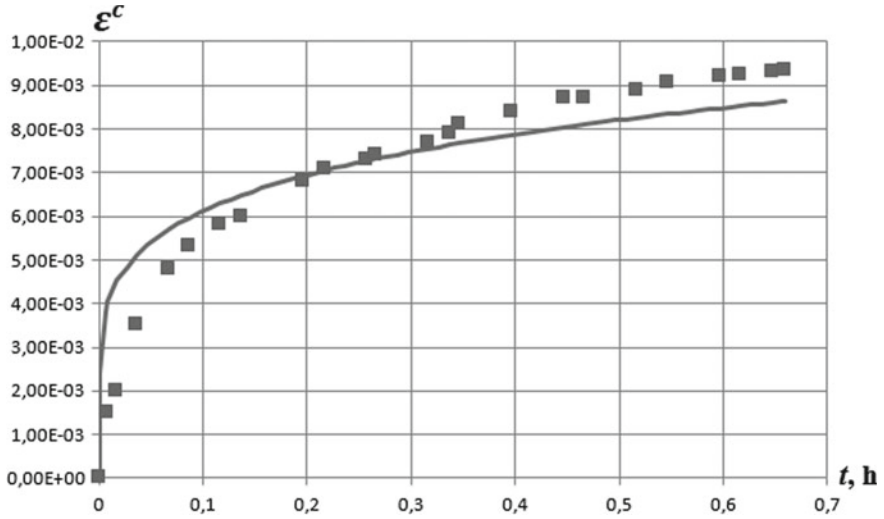

Fig. 10 Comparison of experimental and finite element results (periodic load, transverse direction)

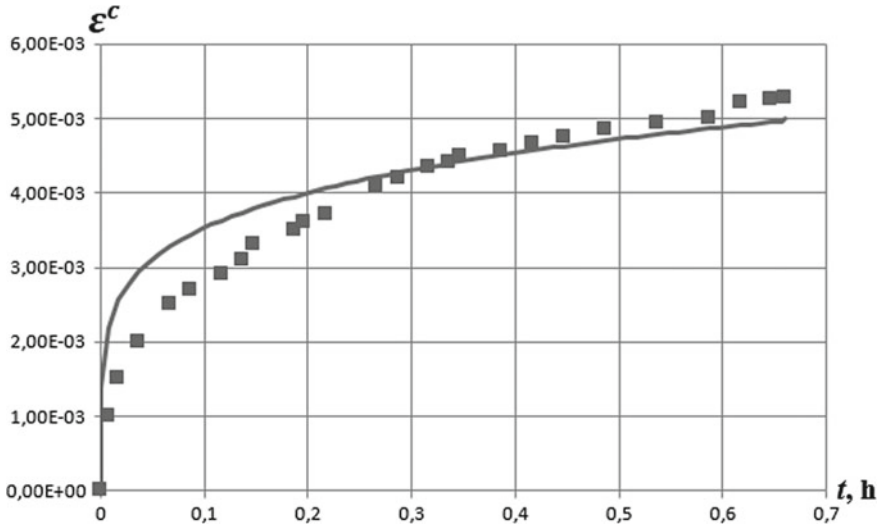

Fig. 11 Comparison of experimental and finite element results (periodic load, direction at an angle of 45° to the rolling direction)

the accuracy of modeling of one-dimensional experiments and two-dimensional calculation schemes can be considered quite satisfactory.

5 Short-Term Creep of Plates with Holes. Experimental Investigations

From the sheets of steel 3 (same material that was used for producing plane specimens) rectangular plates with dimensions 160 × 34 mm were cut out. Each plate was made with 5 holes: one central with diameter 10 mm, and four lateral ones with a diameter 8 mm. Such a scheme was chosen to implement at certain plate's points the stress state, which corresponds to the range of values from creep experiments in specimens. Plates were cut from sheets along the rolling direction. To fix the plates in the AIMA-5-2 test machine, which is designed for tensile testing in creep conditions, the upper and lower technological holes with a diameter of 10 mm were made. The sheme of the plate is shown in Fig. 12. Seven plates were produced. A measuring grid with a step in the longitudinal direction of 1 mm, and with step of 2 mm for transversal one was mechanically added. Video recording was used to obtain data for different moments of time.

The plates with 5 holes were tested at static and periodic tensile loading. In the latter case the program of experiments included partly periodic unloading and loading. Three plates were tested at static loading as well as 4 at periodic. Results of measurements were averaged.

At first let us consider the case of static load. Plates were loaded by weight of 3000 kg (which is equal to tension stress 135 MPa in plate's net section is far from loading hole) during 60 s. Experimental results for different time moments are shown in Fig. 13a–c. From the analysis of photographs it is evident that there is a significant plate's deformation over the time, when circular holes turned into elliptic, and with decreasing the width of the plate in the vicinity of their location. After an instantaneous growth of the strains, their increasing continues in time.

The numerical data of the deformed state were determined by analyzing the resizing of the cells of the dimensional grid. Moment of time t = 3 s was considered as the moment of obtaining plastic strains, then the data was analyzed with time steps up to the moment t = 30 s. We did not succeed experimentally with a satisfactory accuracy to determine the change in the values of displacement $u\,(x, y)$ in the direction x, which is transverse the direction of tension. Thus, the longitudinal displacements $v(x, y)$ were analyzed.

Below, we give the data defined by the measurements in some points of the plates, in which there was the most significant strain increasing (Fig. 14). The data were averaged for three plates. Due to the symmetry of the holes, the data for the left and right halves were also analyzed and added for averaging.

Figure 14 shows the location of the points in which measurements were made for different moments of time. Such points were chosen in the regions on the borders

Fig. 12 Plate with 5 holes

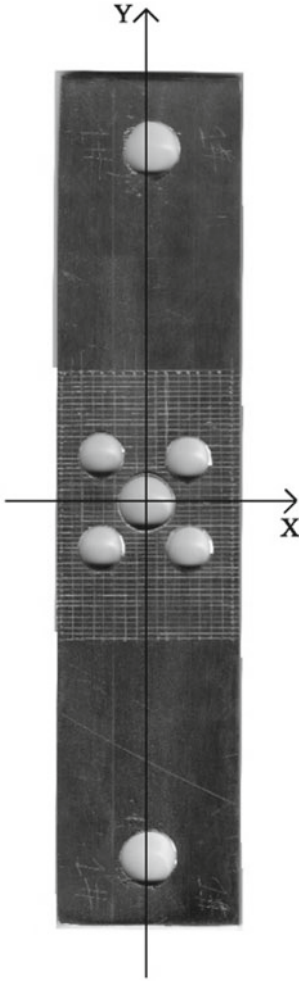

of holes and between them, where the the most significant change in the grid was determined.

Experimental data of varying the displacements in time are shown in Fig. 15, where the points indicate the measured values. The analysis of the obtained results shows the correspondence of character of the curves running in the case of primary creep. Also, let us note their similarity to the curves obtained for specimens in uniaxial tests.

As can be seen from Fig. 15, all the curves for the plate points are qualitatively similar: they have first rapid growth regions at first 20 s, and then their rates decrease. The curve 3 is an exception. It was built for point A, located at the boundary of the

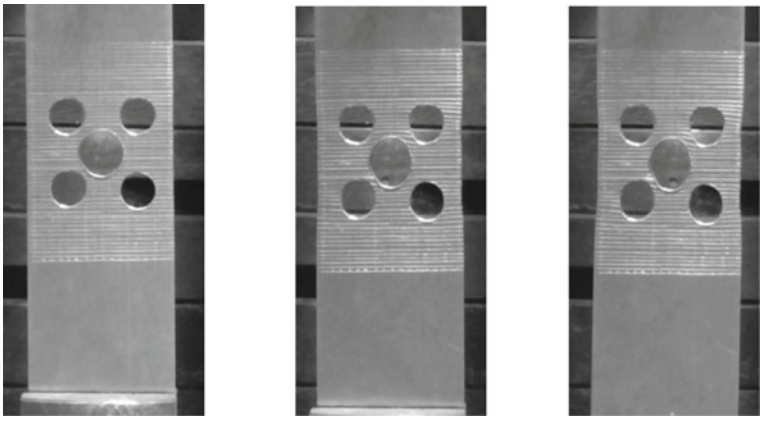

Fig. 13 Deformed plate at static load at different moments of time

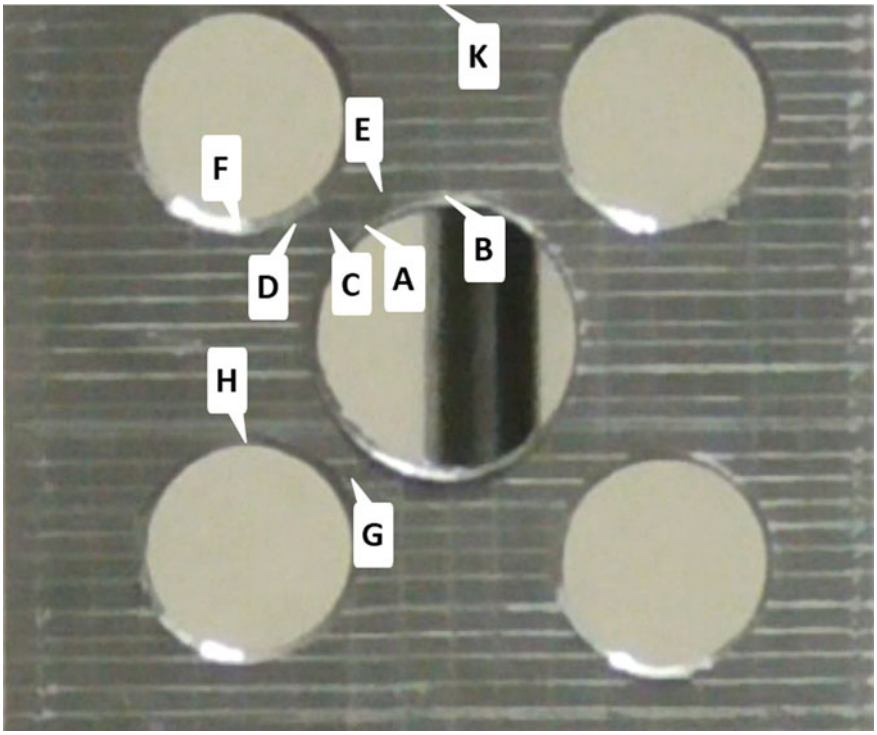

Fig. 14 The location of the plate points in which the measurements of displacements were done (t = 0 s)

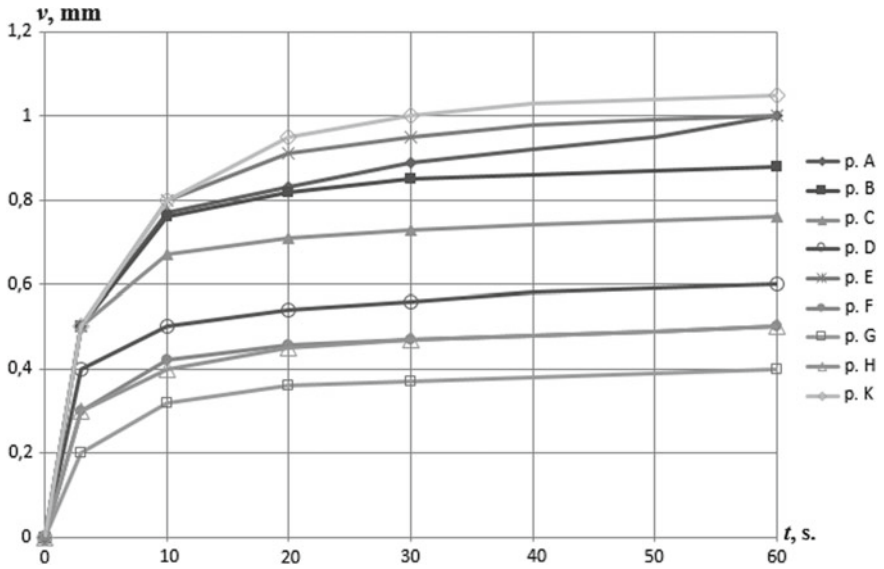

Fig. 15 Varying in time of displacements at the points of the plate, marked by symbols in Fig. 14 (static load)

Fig. 16 Periodic load of plates with holes

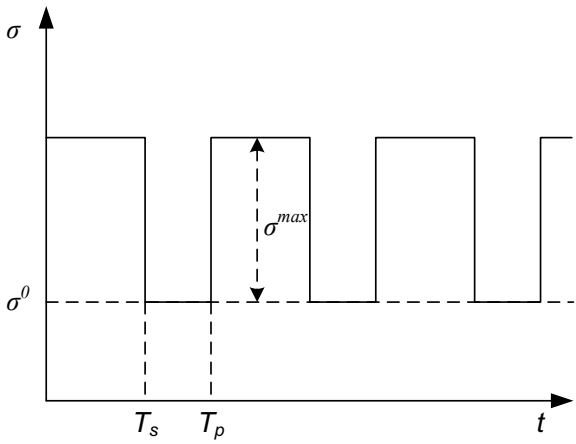

central hole, in which at approximately 50th second, the acceleration of creep begins. According to these data, it is possible to conclude that in this moment the beginning of the third section of the creep curve takes place. It corresponds to accelerated creep, accompanied by a hidden damage. As is well known [3], just in this area, the stress concentration takes place and creep fracture occurs.

Next, we consider the results of an experimental study of the deformation of plates during periodic (cyclic) loading according to the scheme of Fig. 16.

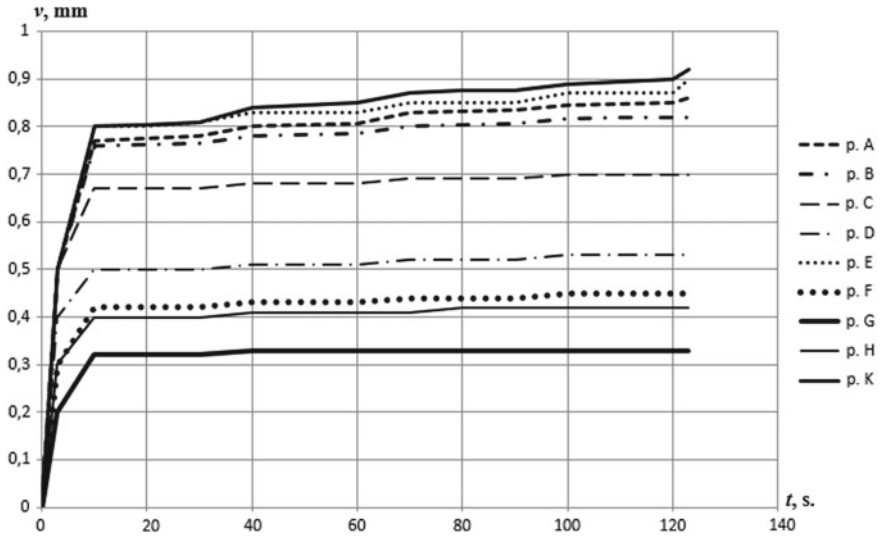

Fig. 17 Varying in time of displacement at the points of the plate, marked by the symbols in Fig. 14 (periodic load)

It was given as follows: for the time $T_s = 10$ s the plate was loaded by stress 135 MPa, as well as next 20 s by stress 121.5 MPa, thus $T_p = 30$ s. During the experiments, it became clear that on the fifth load cycle there was a fracture of the plates in the area of the technological hole designed to organize the load. However, in the areas of transition from the central hole to the small one, as well as from the small hole to the side of the plate, there was a characteristic clouding of the metal, which may indicate a significant damage and close fracture in these places [3, 27]. The analysis of character of deformation showed that there were no fundamental differences in strain running in comparison with experiments at static loading.

Let us consider the results of measurements of longitudinal plate displacements. To obtain this data, a technique similar to that discussed above for static loading was used. Data of measurements obtained by video processing of experiments, for the same points of the Fig. 14 are shown in Fig. 17.

As can be seen from Fig. 17, all obtained curves for plate points are qualitatively similar: with growth in the first 10 s the curves correspond to the curves of purely static load, further due to partial unloading there is a significant deceleration of the growth of displacements.

When plotting the time dependence for longitudinal displacements (Fig. 17), their changes during periods of cycles with lower load values (from 11th to 30th s) were fixed only at points A, B, E, and K, in which maximal displacements took place also in the static experiments. At other points, varying of displacements in the indicated parts of the periods was so small that it could not be determined. It can be explained by the limitations of measurement technique.

As it was already noted, in the places of transition from the central to the lateral holes, characteristic changes of the metal were found, which can be regarded as a evidence of close fracture. This conclusion is also confirmed by the graphs of displacement for those points A and E located in those places. It these points starting from 120th s the accelerated growth of displacement was experimentally obtained.

In general, according to results of experiments with periodic loading of plates it is possible to conclude that there is a significant slowdown in the growth of displacements compared with creep at static loading. The reason is partly unloading. So, for example, at point A for 60 s the value of static displacement is 1 mm, and with a periodic load −0.8 mm; at point E for 60 s. also it is equal 1 mm, and with periodic loading −0.85 mm.

6 Short-Term Creep of Plates with Holes. Numerical Simulation

The results of experimental studies of the deformation of a plate with five holes were compared with numerical data have been obtained by use the developed method and software. As a result of the load's and plate's symmetry, a half-plate model of 17 × 160 mm was used as a calculation scheme, and the plate on the upper side was considered to be loaded with a uniform tension load p = 135 MPa (Fig. 18a). The exact loading of the plate through the hole was also simulated numerically. The lower boundary of the plate was considered to be rigidly fixed. The calculation scheme of the plate with the finite element grid, numbering 838 nodes and 1474 elements, is shown in Fig. 18a. This grid was selected after preliminary elastic-plastic calculations that were performed both in the *FEM CREEP* software and in *ANSYS* with the same grids. It was established that the stress state is determined approximately the same, with a difference of 10–15 MPa and qualitatively close zones with the same level of stress. Distribution of von Mises stress is shown in Fig. 18b. The results of the calculations show a significant stress concentration in the zones between the holes and at an angle of approximately 45° to the holes in the directions to the outer sides of the plates, the maximum value of von Mises stress is 394 MPa, which is close to the material strength limit of 395.3 MPa.

Further, the modeling of the plate's creep for 30 s was considered. In the calculations, the values of creep constants of the plate material, obtained by experimental data processing, were used. Numerical simulations are carried out with a variable integration step, from the initial value of 1×10^{-9} to 1×10^{-4} h.

The results of calculations using the *FEM CREEP* software were compared with the data obtained after processing the video of experiments. Let us consider the results of this comparison. The data of the deformation of plates near holes, where a two-dimensional stressed state is realized, are analysed. The measurements were compared for different moments of time up to 30 s. The values of the displacement components v, mm were compared with the values obtained for the corresponding

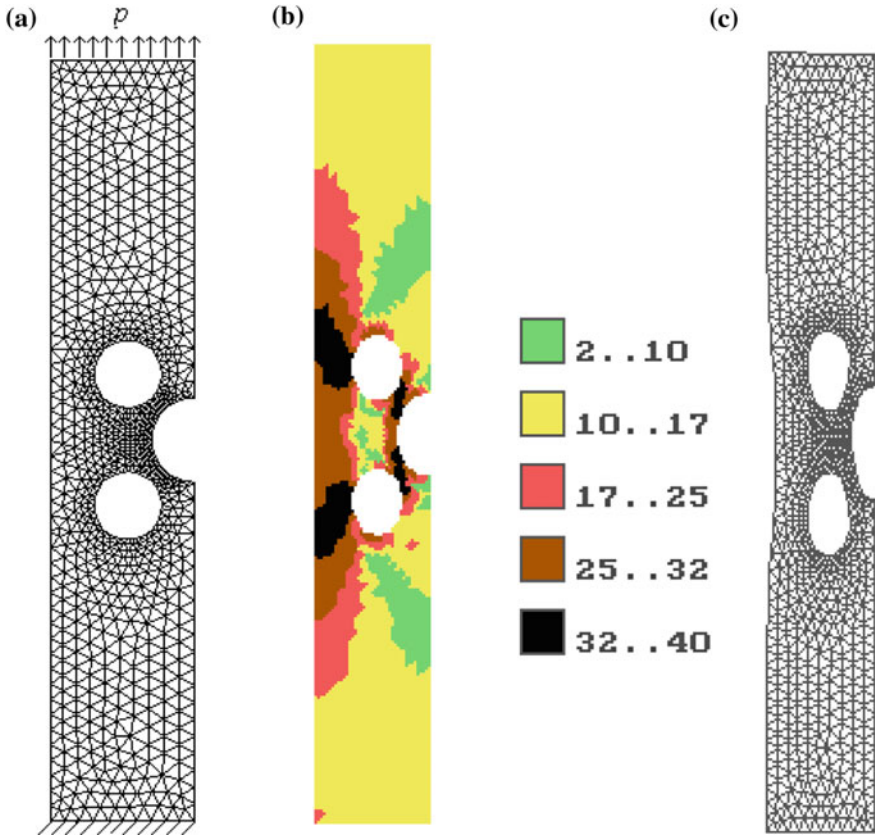

Fig. 18 FE model of the half of a plate (**a**), initial von Mises stress distibution, $\sigma_{vM} \cdot 10^{-1}$MPa (**b**) and deformed FE mesh, t = 30 s, scale 1:60 (**c**)

nodes of the finite element grid. The displacement components u with a given deformation pattern have significantly lower values that could not be determined by the used method of grids comparison.

A finite element grid, which is deformed due to calculation data for the time t = 30 s, is presented in Fig. 18c. Comparing it with Fig. 13b, where the photo of the deformed plate is located for the same moment, allows us to draw a conclusion on a qualitatively correct description of deformation under creep.

Let us consider quantitative estimates. Table 1 shows the results of the comparison of experimental and numerically determined values of short-time creep displacement for points located between the three holes in which there is a significant deformation under creep running. The locations of points marked with symbols are presented in Fig. 14. These points in finite element model correspond to the numbers of nodes, shown in Fig. 19. Point K corresponds to the 424th node, which due to the applied scale is not shown in Fig. 19.

Table 1 Comparison of experimental and numerically determined displacements [mm] for t = 30 s

Point/ Node number	A/ 44	B/ 37	C/ 270	D/ 286	E/ 250	F/ 169	G/ 258	H/ 194	K/ 424
Experimental data	0.4	0.35	0.23	0.15	0.45	0.17	0.17	0.17	0.5
Numerical data	0.32	0.34	0.25	0.21	0.3	0.2	0.13	0.19	0.34
Error, %	20	3	9	29	33	15	24	11	32

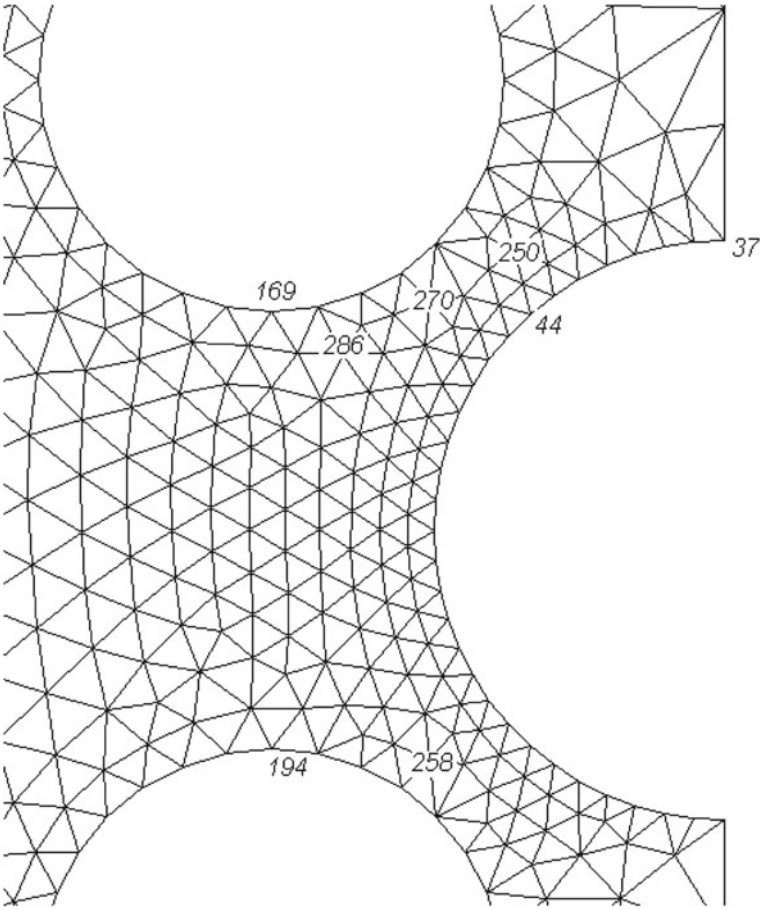

Fig. 19 Location of nodes of a finite element grid near three holes

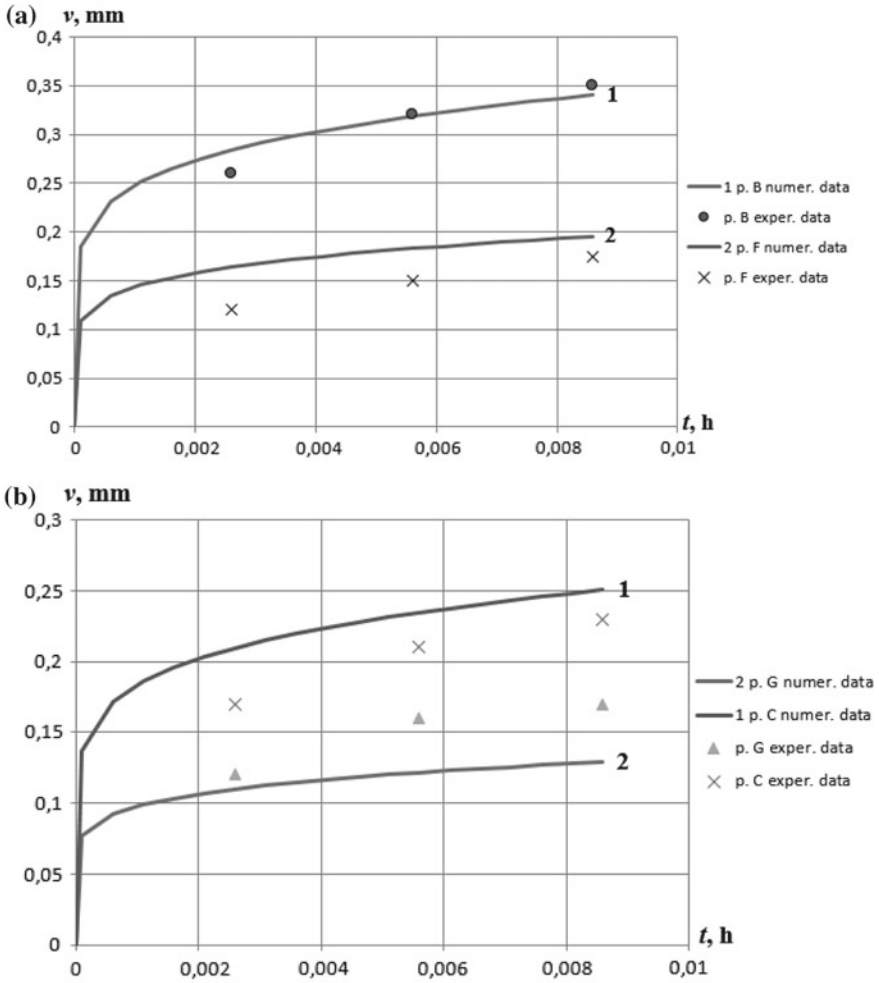

Fig. 20 Displacements versus time in points B, F (**a**) and in points C, G (**b**)

Analysis of the data from Table 1 shows that in the regions with the highest displacement level, the maximum difference between numerical and experimental data is 32–33%, but at other points, the errors are much lower.

Comparison of numerical (solid lines) and experimental data (points) for different moments of time is shown in Fig. 20.

Analyzing the data of Fig. 20, which gives a comparison the displacement's calculation and experimental data at different points of the plate, we conclude that numerical simulation qualitatively reflects the process of deformation in time. Quantitative differences range from 3 to 40% for various plate fragments. The latter value

Table 2 Data on the stress redistribution in the vicinity between two holes, σ_i, MPa

№ el.	1324	1309	1340	1361	1381	1404	1405	1429	1430	1454	1455
$t = 0$ s	254	268	331	332	340	338	349	340	367	358	385
$t = 30$ s	322	301	334	333	348	330	331	317	306	298	313

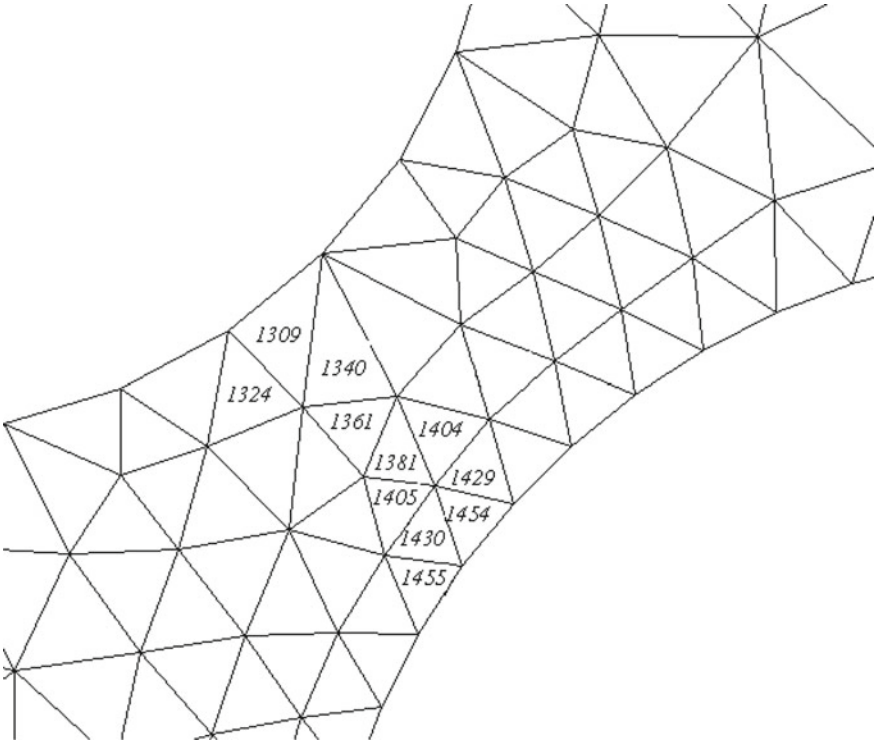

Fig. 21 The location of the elements for Table 2 in the applied finite element grid

is quite large, but it must be taken into account that the experimental data are also determined with a certain error in the measurement.

Numerical simulation of the short-term creep of the plate also provides a qualitatively correct estimate of stress varying: there is a redistribution of stresses in the vicinity between the holes, and between the holes and free side of the plate. The qualitative character of the stress distribution does not change, and the most loaded zones remain the same. As an example, let us consider the data of stress redistribution in the zone between two holes (Table 2). The elements selected for comparison are located between the upper and central holes, their numbers are shown in Fig. 21. In the table, the elements are given starting with numbers at the upper holes and finishing at the lower ones.

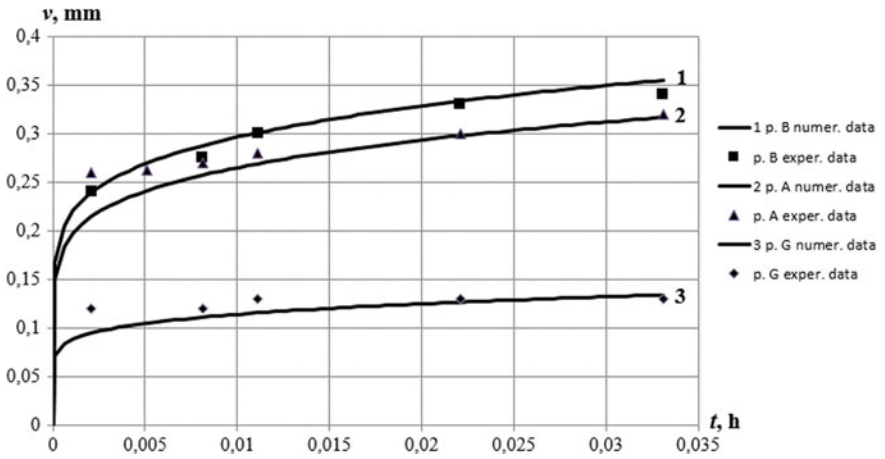

Fig. 22 Comparison of numerical and experimental data (periodic load, points A, B and G)

It is evident from the analysis of Table 2 that for a short period of time (30 s) there is a certain redistribution of von Mises stresses in the area between the holes. Near the central hole there is a relaxation (from 385 to 313 MPa), and near the upper one a certain growth presents.

Next, let us consider the periodic loading of these plates, comparing the experimental and numerical creep results. According to the analysis of experimental data, it can be seen that for comparison it is possible to use the data for four load cycles of 2 min. If you analyze the data shown in Figs. 4, 9, 10 and 11, you can see that 4 is the limiting value of the cycles number, in which in uniaxial case the values with a satisfactory error are obtained. Unfortunately, the peculiarities of the experiment and the creep properties of used steel 3 did not provide the opportunity to increase the number of cycles.

The analysis of the experimental study of creep of the considered plates shows that there is no qualitative difference between the distribution of displacement and the running of the deformation process in the case of static and periodic loading. In this regard, as an example, we give in Fig. 22 only data from the comparison of experimental and numerical results in some characteristic points (Fig. 14), selected for analysis. Point B corresponds to the zone with maximum displacements, point A is a characteristic point for the zone between the upper holes, and point G is located between the lower ones. The calculated data are presented in Fig. 22 by solid lines and the points correspond to experimental results. Experimental data for point A is indicated by triangles, for a point B by squares, and for a point G by diamonds.

As can be seen from the results of the comparison, the varying of displacements in creep process at complex two-dimensional stress state is qualitatively correctly described by the calculated data. Their form, similar to the case of static loading, corresponds to the form of primary creep cyrves. Reducing the creep rate compared

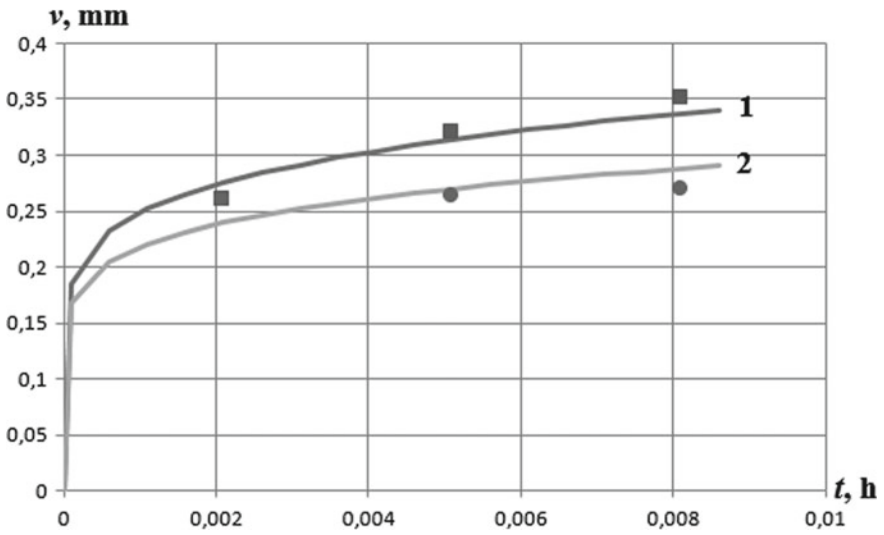

Fig. 23 Comparison of calculated and experimental data for static and periodic loads (point B)

to the static load data, which takes place due to the load decreasing in the second part of the period, is also described qualitatively correct.

Maximum error between numerical and experimental data was determined for the first 10 s at all points, and the largest (at the point G) is 35%. The values for 120 s. (at points C and F) are 25% and 27% respectively. The creep rate, which can be analyzed by the slope of the curves, is evaluated satisfactorily, with an error of 10–15%. As can be seen from the figures, there is an overestimation for numerical data for the first periods. This can be explained by not very exact measurement technique, but also by the insufficient number of load cycles for completely satisfactory experimental conditions, which would require their greater number.

A comparison between calculated displacement curve at point B for cases of static (curve 1) and periodic loading (curve 2) is presented in Fig. 23. As can be seen from the graph, the errors are not very big. For the first ten seconds the experimental points coincide, this occurred because in both cases the loading is the same. Differences of 5–8% between the numerical and experimental data are much smaller than the difference of 30% between the data of static and periodic loading, which can demonstrate the possibility of numerical determination of the influence of periodic loading effect in the complex stress state.

Numerical studies which were done, comparison of their results with experimental data, obtained at the same time with a sufficient error degree, provides the opportunity to use the developed software for solving the practical problems.

7 Conclusions

The chapter provides a description of the method for solving the plane creep problems for structural elements made of materials with transversally isotropic creep properties. The case in which the instantaneous load leads to the appearance of plastic deformations is considered.

The creep law for the case of periodic loading at primary short-term creep for cases of uniaxial and plane stress states is experimentally verified. The values of the constants for the equation describing the transversally isotropic creep are obtained. It is established that:

- the creep curves in all directions (along the width, across and at an angle of 45º to the direction of rolling) of steel sheets are similar;
- the maximum creep rate is realized in the direction along the rolling, and the minimum takes place at the direction determining by an angle of 45° to rolling; the form of the creep curves corresponds to the primary creep;
- the main part of the deformation is obtained in the first minutes of creep, which gives the possibility to classify the curves by the type of short-term creep;
- creep almost stops after 30 min of deformation.

The verification study of the calculated method was carried out by comparing the numerical and experimental results of uniaxial and plane stress conditions that occurs in investigated plates with five holes. The satisfactory for physically nonlinear two-dimensional problems deviation of calculated and experimental data within the limits of 25–30%, with the exception of two points in the case of periodic loading, in which the level of displacement is smaller than more than twice as much as the maximum, is found. The difference may be explained by the measurement technique.

The proposed method for the periodic load case due to its similarity to the standard method for static problems as well as due to decreasing of calculation time can be recommended for the analysis of practical problems with the similar forms of the cycle, which number has not be less than four.

References

1. Lemaitre, J., Chaboche, J.-L.: Mechanics of Solid Materials. Cambridge University Press, Cambridge (1994)
2. Rabotnov, YuN, Mileyko, S.T.: Short-term Creep. Nauka, Moscow (1970). (in Russ.)
3. Rabotnov, YuN: Creep Problems in Structural Members. North-Holland, Amsterdam (1969)
4. Malinin, N.N.: Applied Theory of Plasticity and Creep. Mashinostroenie, Moscow (1975). (in Russ.)
5. Hoff, N.J.: Structures and materials for finite lifetime. Adv. Aeronaut. Sci.: Proc. First Int. Congr. Aeronaut. Sci. **2**, 928–961 (1959)
6. Kassner, M.E.: Fundamentals of Creep in Metals and Alloys. Elsevier Science Technology, London (2015)
7. Nikitenko, A.F., Sosnin, O.V.: Creep and long-term strength under cyclic loading conditions. Strength Mater. **8**, 1395–1398 (1976)

8. Stryzhalo, V.O.: On the applicability of creep theories and methods of estimating durability for case of stepped directed deformation of material in a low-cycle region. Proc. Acad. Sc Ukr. **3**, 14–24 (1978). (in Ukrain.)
9. Lebedev, A.A., Giginyak, F.F., Bashta, V.V.: Cyclic creep of body steels under a complex stress system in the temperatures range 20–400 C. Strength Mater. **10**(10), 1128–1131 (1978)
10. Kennedy, A.J.: Processes of Creep And Fatigue in Metals. Wiley, London (1963)
11. Tsimbalistyi, Ya.I., Troyan, I.A., Marusii, O.I.: Investigation of the vibrocreep of alloy EI437B at normal and high temperatures. Strength Mater. **7**, 1331–1335 (1975)
12. Weinbel, R.C., Schwarzkopf, E.A., Tien, J.K.: Effects of frequency on the cyclic creep and fracture of a lead-rich-lead-tin solder alloy. Scr. Metall. **21**, 1165–1168 (1987)
13. Fakpana, K., Otsukab, Y., Mutohb, Y., Inouec, S., Nagatad, K., Kodani, K.: Creep-fatigue crack growth behavior of Pb-contained and Pb-free solders at room and elevated temperatures. Procedia Eng. **10**, 1238–1243 (2011)
14. Wagoner, R.H., Chenot, J.L.: Metal Forming Analysis. Cambridge University Press, Cambridge (2001)
15. Saanouni, K., Chaboche, J.-L.: Computational damage mechanics: application to metal forming simulation. Compr. Struct. Integr. **3**, 321–376 (2003)
16. Saanouni, K.: Damage Mechanics in Metal Forming: Advanced Modeling and Numerical Simulation. Wiley, London (2012)
17. Breslavskii, D.V., Morachkovskii, O.K.: Nonlinear creep and the collapse of flat bodies. Int. Appl. Mech. **34**(3), 287–292 (1998)
18. Breslavsky, D., Morachkovsky, O., Tatarinova, O.: Creep and damage in shells of revolution under cyclic loading and heating. Int. J. Nonlinear Mech. **66**, 87–95 (2014)
19. Breslavskii, D.V., Metelev, V.A., Morachkovskii, O.K.: Anisotropic creep and damage in structural elements under cyclic loading. Strength Mater. **47**(2), 235–241 (2015)
20. Hamming, R.W.: Numerical Methods for Scients and Engineers. McGraw-Hill, New York (1973)
21. Moiseev, N.N.: Asymptotic Methods of Nonlinear Mechanics. Nauka, Moscow (1969). (in Russ.)
22. Breslavsky, D.V., Konkin, V.M., Mietielov, V.O.: Plasticity and creep of steel 3 at room temperature. Bull. NTU "KhPI". Ser.: Dyn. Strength Mach. **46**(1218), 77–81 (2016)
23. Chaboche, J.-L.: A review of some plasticity and viscoplasticity constitutive equations. Int. J. Plast. **24**, 1642–1693 (2008)
24. Breslavsky, D.V., Korytko, Yu. N., Tatarinova, O.A.: Design and Development of Finite Element Method Software. Kharkiv: Pidruchnyk NTU « KhPI » . (in Ukrain.) (2017)
25. Zienkiewicz, O.C., Taylor, R.L., Wood, D.D.: The Finite Element Method for Solid and Structural Mechanics. Butterworth-Heinemann (2014)
26. Bathe, K.J.: Finite-Elemente Methoden. Springer, Berlin (1990)
27. Walczak, J., Sieniawski, J., Bathe, K.: On the analysis of creep stability and rupture. Comput. Struct. **17**(5–6), 783–792 (1983)